J Mater Sci (2009) 44:3793–3799
DOI 10.1007/s10853-009-3511-y

On the metastable miscibility gap in liquid Cu–Cr alloys

Z. M. Zhou · Jianrong Gao · F. Li · Y. K. Zhang · Y. P. Wang · M. Kolbe

Received: 16 February 2009 / Accepted: 22 April 2009 / Published online: 6 May 2009

Abstract Electromagnetically levitated Cu–Cr alloy melts containing 5–70 at.% Cr were splat-quenched onto a chill substrate. The microstructure of the solidified alloys was investigated by scanning electron microscopy. The alloys containing 5–60 at.% Cr showed a droplet-shaped microstructure consisting of Cr-rich spheroids or and dendrites in a Cu-rich matrix, whereas those containing 65 and 70 at.% Cr showed a banded microstructure consisting of alternative Cu-rich and Cr-rich bands. Both types of microstructure presented evidence for metastable phase separation in Cu–Cr alloy compositions, thus verifying the existence of a broad miscibility gap in the undercooled liquid. However, the results suggested that the miscibility gap has a Cr-rich critical composition and a skewed geometry.

Z. M. Zhou · J. Gao (✉) · F. Li · Y. K. Zhang
Key Laboratory of Electromagnetic Processing of Materials (Ministry of Education), Northeastern University, Shenyang 110004, China
e-mail: jgao@mail.neu.edu.cn

Z. M. Zhou · Y. P. Wang
Institute of Metal Research, Chinese Academy of Sciences, Shenyang 110016, China

M. Kolbe
Institut für Materialphysik im Weltraum, Deutsches Zentrum für Luft- und Raumfahrt (DLR), Köln 51170, Germany

Y. P. Wang
Department of Materials Physics, Xi'an Jiaotong University, Xi'an 710049, China

Introduction

Cu–Cr alloys have found many applications because they exhibit an excellent combination of high mechanical strength with high conductivities, both thermal and electrical. Numerous studies have been devoted to an understanding of the relationship between microstructure and performance of the alloys prepared by various methods. However, there has been a discrepancy with regard to the type of the phase diagram [1–11]. The pioneer study by Hindrichs [1] as well as a number of following studies [2–4] have suggested a monotectic-type phase diagram, in which a stable miscibility gap existed at Cr-rich alloy compositions. Such a type of phase diagram has been generally questioned, and related to an impurity effect resulting from the use of impure raw materials and a reactive atmosphere. The currently accepted Cu–Cr phase diagram was proposed by Jacob et al. [11] following a thermodynamic study of the system using the Knudsen cell-mass spectrometry. It falls into the category of simple eutectic, but includes a metastable miscibility gap in the undercooled liquid. Under the assumption of a pseudo-subregular solution model, those researchers calculated the metastable phase boundaries of the system, and predicted that the miscibility gap has a critical composition of 43.6 at.% Cr at 1787 K and expands considerably at lower temperatures. Due to the existence of the metastable miscibility gap, it is expected that an initially homogeneous bulk alloy will be separated into a mixture of a Cr-rich liquid and a Cu-rich liquid, providing a composition-dependent critical undercooling is achieved. In literature, liquid phase separation actually has been suggested for rapidly solidified alloy compositions based on observations of a droplet-shaped solidification microstructure consisting of a dispersion of fine Cr-rich spheroids in a Cu-rich matrix

[12–14]. Although such observations generally agreed with the study by Jacob et al. [11], the boundaries of the calculated metastable miscibility gap have not been fully checked. On the one hand, most of rapid solidification experiments were performed on Cu-rich alloy compositions, leaving liquid phase separation in Cr-rich alloy compositions unexplored. On the other hand, bulk alloys for rapid solidification experiments were all melted in a ceramic crucible, which, however, caused melt contamination, as evidenced by the formation of impurity particles in melt-spun ribbons [14]. So far, little attention has been paid to this issue, though the impurities have been assumed to be responsible for the observation of the stable miscibility gap in earlier studies of the system [1–4]. For the two reasons, more investigations are required for a full test of the calculated miscibility gap.

In a previous study [15], a Cu-rich alloy composition was electromagnetically levitated in an attempt to determine the critical undercooling for triggering of the metastable phase separation. Unexpectedly, the formation of a Cr_2O_3 oxide layer on the sample surface upon gas cooling led to a poor undercooling and therefore to a dendritic microstructure. However, a droplet-shaped microstructure similar to that of melt-spun ribbons was observed for samples electromagnetically levitated and subsequently splat-quenched onto a chill substrate, thus suggesting liquid phase separation prior to rapid solidification. Due to avoidance of the crucible-induced melt contamination, the splat-quenched samples did not include the impurity particles, which were identified for the melt-spun ribbons. It was suggested that the combination of electromagnetic levitation with splat-quenching may serve as an alternative method for a test of the calculated miscibility gap of the Cu–Cr system in a clean environment. In the present study, the method was extended to a wide range of Cu–Cr alloy compositions including several Cr-rich ones, aiming at verification of the critical composition and width of the miscibility gap.

Experimental

Master alloys of atomic composition $Cu_{100-x}Cr_x$ ($x = 5$, 10, 15, 20, 25, 30, 35, 40, 45, 50, 55, 60, 65, and 70) were prepared by arc-melting electrolytic Cu and Cr sheets of 5 N purity under a Ti-gettered atmosphere. An excess mass of elemental Cu was added to compensate for mass loss during melting. The alloys were all melted several times, and had a mass of 1.5–1.8 g finally. An alloy was positioned in a radio frequency levitation coil with an alumina-made sample holder. After being evacuated to a vacuum pressure of 6×10^{-4} Pa, the levitation chamber was backfilled with pure argon (5 N purity) to a pressure of 3×10^4 Pa. The sample was levitated and melted inductively. The sample temperature was monitored with a single-color pyrometer, which was aligned coaxially with the levitation coil through a quartz view port. For Cr-rich alloy compositions, a dense metal vapor appeared over the top surface of the levitated samples, and reduced the intensity of radiation detected by the pyrometer. For calibration, the temperature of the molten samples was also measured with the same pyrometer through a horizontal view port of the levitation chamber. A maximum shift of 300 K was determined for the highest Cr alloy composition ($x = 70$), whereas no shift was determined for low Cr alloy compositions ($x = 5$–15). After keeping for few minutes, the sample was released from the levitation coil by cutting off the power suddenly. The sample was splat-quenched against a polished copper plate at a distance of 20 cm below the coil. The quenched sample was spread on the chill substrate, and cast into a disk-like geometry of a larger thickness at the edge than at the center. In few experiments, a hat-like geometry of a larger thickness at the center than at the edge was cast as a result of incomplete melting of the levitated sample. Only the samples of the disk-like geometry were analyzed in the present study. They were mounted in a resin and polished. Their transverse microstructure was examined using a scanning electron microscope (SEM) equipped with an energy dispersive X-ray spectrometer (EDS). The oxygen concentration of the samples was analyzed using the combustion method.

Results

Figure 1 illustrates the recorded pyrometer signals of the splat-quenched samples. A comparative analysis of the signals led to an assumption that all of the samples had experienced a four-staged cooling process: (1) radiation-dominating natural cooling during free fall of the liquid samples, (2) rapid cooling of the liquid samples in intimate contact with the chill substrate, (3) negative cooling, i.e., recalescence, of the semi-solid samples during rapid solidification, and (4) post-solidification cooling of the fully solid samples. Because of a relatively long response time of the order of tens of milliseconds as well as a lower detection limit of 1023 K, the pyrometer might have missed one or more cooling stages of the samples. For example, it missed the last two cooling stages of two low Cr samples. In addition, as mentioned above, the dense metal vapor rising from the top surface of high Cr samples reduced the intensity of the pyrometer signal, leading to a large deviation of the measured temperature from the real value. Despite such imperfections, the pyrometer signals shown in Fig. 1 released critical information about cooling

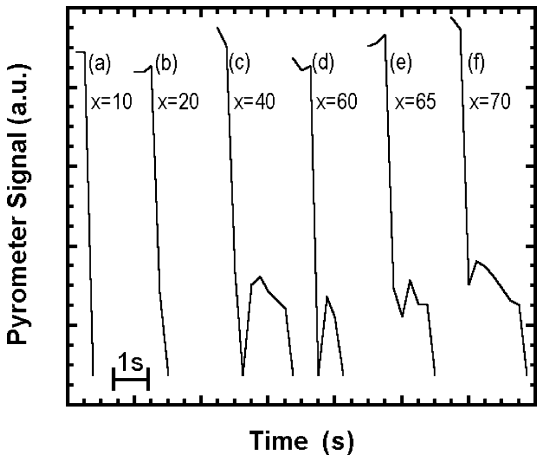

Fig. 1 Illustration of recorded pyrometer signals of $Cu_{100-x}Cr_x$ samples. The signals for high Cr alloy samples were shifted to low values due to the formation of a dense metal vapor along the view path of the pyrometer

and solidification of the splat-quenched samples. From those of the low Cr samples, a cooling rate of the order of 1000 K/s was estimated for the second stage of the cooling process, which agreed with that reported for splat-quenched pure Ni samples [16]. The high Cr samples might have experienced a higher cooling rate than that of the low Cr samples at the first stage because of a higher liquidus and a larger emissivity as well. But, they might have experienced a lower cooling rate at the second stage because of a lower Cu concentration and therefore a lower thermal conductivity. More critically, the pyrometer signals of some samples recorded a strong recalescence event at the negative cooling stage. It was implied that those samples had reached a large undercooling by rapid cooling. Owing to a comparable cooling rate at the second cooling stage, other samples had also reached a large undercooling, but the subsequent recalescence event might have been missed by the pyrometer for the reasons mentioned above.

SEM investigations showed that the microstructure of the samples depended on alloy composition. As shown in Fig. 2, a droplet-shaped microstructure consisting of Cr-rich spheroids in a Cu-rich matrix was observed in common for alloy compositions with $x = 5$–60 at.% Cr. In the transverse section of the samples, the size of the Cr-rich spheroids was increased with increasing distance from the chill substrate, whereas their density per unit area was decreased. The observation of such a non-uniform distribution of the density and size of the Cr-rich spheroids agreed with the previous studies [14, 15]. For different alloy compositions, the droplet-shaped microstructure also showed progressive changes with increasing x. As seen in Fig. 2a, the Cr-rich spheroids in the alloys with $x = 5$ were sparse, and had a small size, typically of few hundred

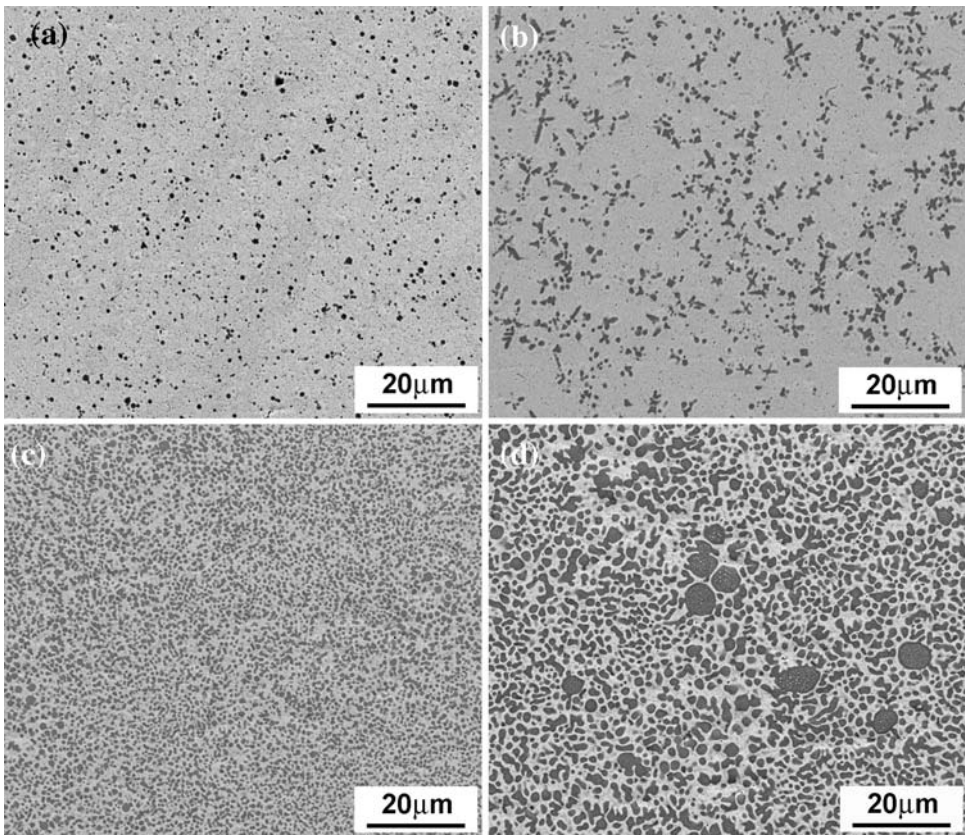

Fig. 2 Back-scattered SEM micrographs illustrating a droplet-shaped microstructure in splat-quenched $Cu_{100-x}Cr_x$ samples. **a** $x = 5$, **b** $x = 15$, **c** $x = 40$, and **d** $x = 50$

nanometers in diameter. In the alloys with $x = 15$, the Cr-rich spheroids remained fine with an increased density. Additionally, as shown in Fig. 2b, Cr-rich dendrites were also formed in the Cu-rich matrix, particularly at the free surface side of the samples. The density of the Cr-rich spheroids was increased continuously with increasing x, till it reached a maximum at $x = 40$ (see Fig. 2c). Increasing x to 45 or above led to significant coarsening of the Cr-rich spheroids, i.e., the size of the Cr-rich spheroids was increased at the expenses of the density. In the alloys with $x = 50$, large Cr-rich spheroids began to decompose, which was evidenced by the observation of a substructure consisting of a dispersion of fine Cu-rich dots in a Cr-rich matrix (see Fig. 2d). Moreover, few of them showed a distorted morphology, looking more like ellipsoids. Such changes in the substructure and morphology of the Cr-rich spheroids became pronounced in the alloys with $x = 55$ and 60. When x was increased to 65, a novel microstructure, termed banded microstructure, was observed. As shown in Fig. 3a, there existed a number of Cr-rich bands, of which the longitudinal directions appeared parallel to the sample surfaces. Under high magnification, the Cr-rich bands were found to have the same substructure as that of the large Cr-rich spheroids, whereas the surrounding material showed the droplet-shaped microstructure as was observed in low Cr samples (see Fig. 3b). In the alloys with $x = 70$, the Cr-rich bands had grown over the whole transverse section, as shown in Fig. 3c. But, their surfaces became uneven. Depending on the location, either shrinkage holes or Cu-rich bands of a shorter length were formed in-between the Cr-rich bands. In local regions, a regular microstructure consisting of alternative Cr-rich and Cu-rich bands was observed, as shown in Fig. 3d. A careful examination found that the long Cr-rich bands actually were segmented by a thin Cu-rich layer, whereas the Cr-rich spheroids in the Cu-rich bands tended to migrate toward the neighboring Cr-rich bands.

As will be explained below, both the Cr-rich spheroids and the Cr-rich bands were considered to be the evidence for the metastable liquid phase separation. Thus, their compositions were analyzed by EDS. The results are summarized in Fig. 4. Owing to the submicron size, the composition of the Cr-rich spheroids in the alloys with $x = 5$–25 were not analyzed. Additionally, the Cr-rich spheroids and bands of the alloys with $x = 65$ and 70 were found to have an identical composition within the error of EDS, and hence, their data were not marked separately. The measured data showed a variable Cr content ranging between 84.8 and 91.8 at.% Cr. But, there was no consistent tendency in sequence of increasing x.

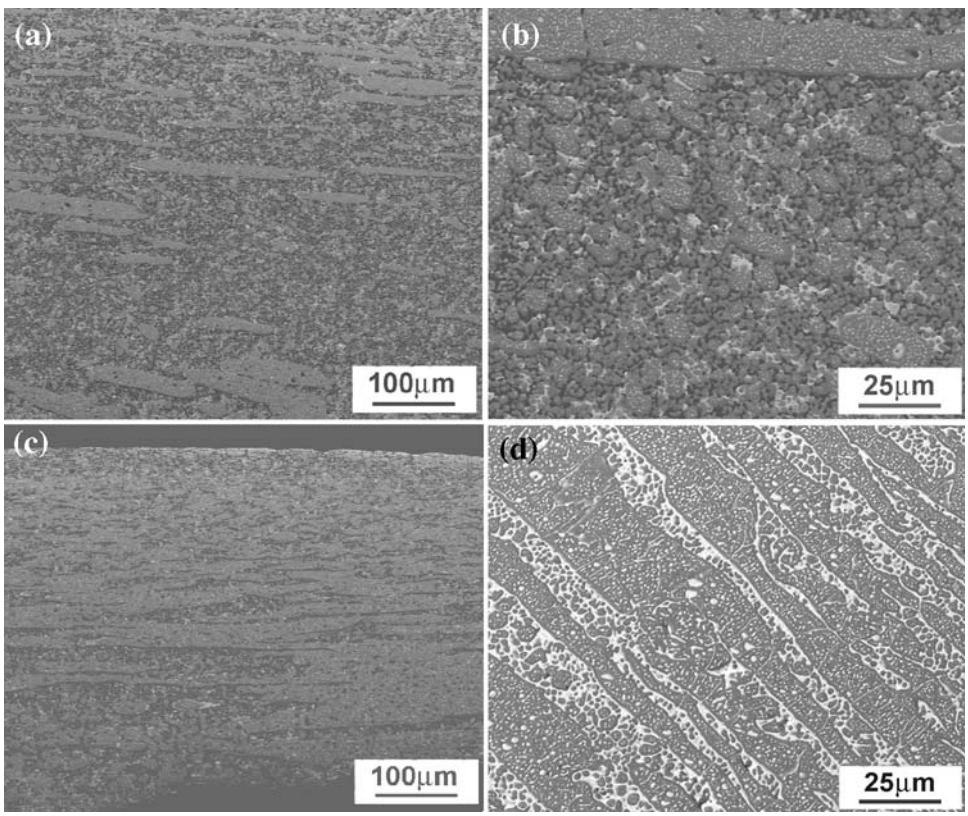

Fig. 3 Back-scattered SEM micrographs illustrating a banded microstructure in splat-quenched $Cu_{100-x}Cr_x$ samples. **a** and **b** for $x = 65$, **c** and **d** for $x = 70$

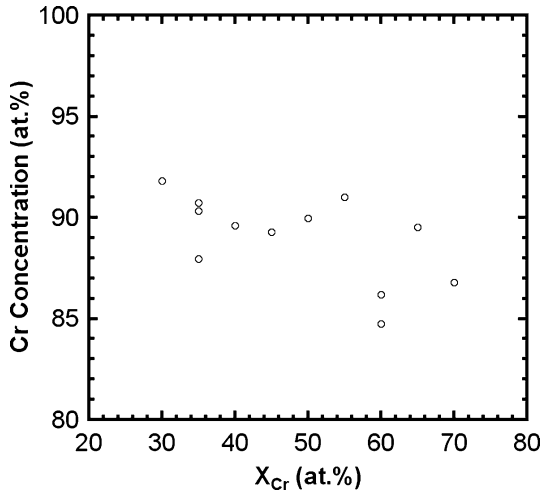

Fig. 4 EDS analysis of Cr content of Cr-rich spheroids and bands in splat-quenched $Cu_{100-x}Cr_x$ samples

Discussion

Width of the miscibility gap

The present samples showed two types of solidification microstructure, a droplet-shaped one and a banded one. As seen in Fig. 1, the whole cooling process of the samples lasted only few seconds. Even if the time for liquid cooling and for recalescence was neglected, such a short interval could not allow nano-sized nuclei of a solid solution to grow to a size of few hundred nanometers due to sluggish diffusion kinetics in the solid state. But, if nano-size Cr-rich droplets were nucleated from a supersaturated liquid solution, i.e., via the metastable liquid phase separation, they would be able to reach a size even of tens of micrometers within a few seconds due to a faster diffusion kinetics as well as collision-assisted coagulation in the liquid state [14]. Hence, the droplet-shaped microstructure of Fig. 2 was assumed to be the direct evidence for the metastable liquid phase separation during splat-quenching. On the other hand, the banded microstructure of the two high Cr samples also suggested the metastable liquid phase separation, because it not only included the same droplet-shaped microstructure in-between the Cr-rich bands (Fig. 3c), but also showed a spatial separation of the bulk samples into interconnected Cr-rich bands and Cu-rich bands (Fig. 3d). Thus, it can be concluded that liquid phase separation occurred to all of the alloy compositions under study. Inversely, it was implied that there exists a broad miscibility gap in the Cu–Cr system, which spans from 5 to 70 at.% Cr. Due to the fact that liquid phase separation is a continuous process [17, 18], the miscibility gap might have been extended at reduced temperatures. In terms of the EDS analysis, the Cr-rich spheroids had a maximum Cr content of 91.8 at.% (see Fig. 4). The value actually corresponded to a composition of the Cr-rich liquid at the end of liquid phase separation, and therefore, marked an accessible Cr-rich boundary of the miscibility gap. In principle, the Cu-rich boundary of the miscibility gap should have also been extended more or less. Due to the dispersion of fine Cr-rich spheroids, the composition of the Cu-rich matrix was not analyzed here. Thus, the miscibility gap was estimated to have a width at least of 86.8 at.% Cr for accessible undercoolings. Such a width agreed fairly well with the calculated miscibility gap, which is reproduced in Fig. 5 showing a width of 87.1 at.% Cr at the equilibrium eutectic temperature. It is thus concluded that the calculated miscibility gap is accurate with respect to the width in low temperature regions.

Critical composition and geometry of the miscibility gap

Note in Fig. 5 that the calculated miscibility gap is approximately symmetric with respect to the critical composition of 43.6 at.% Cr. By application of the lever rule, it can be expected that the phase-separated alloys with $x = 5$–40 will show a dispersion of Cr-rich spheroids in a Cu-rich matrix, whereas those with $x = 45$–70 will show a dispersion of Cu-rich spheroids in a Cr-rich matrix. However, as seen in Figs. 2 and 3, the Cu-rich liquid appeared to be the matrix phase over a wider range of alloy composition, from $x = 5$ to $x = 60$, than expected, whereas the Cr-rich liquid appeared to be the matrix phase for the alloy compositions with $x = 65$ and 70 only. It is evident that there existed a discrepancy between the expected and the real microstructure of middle alloy compositions. In order to explain the discrepancy, a miscibility gap with a

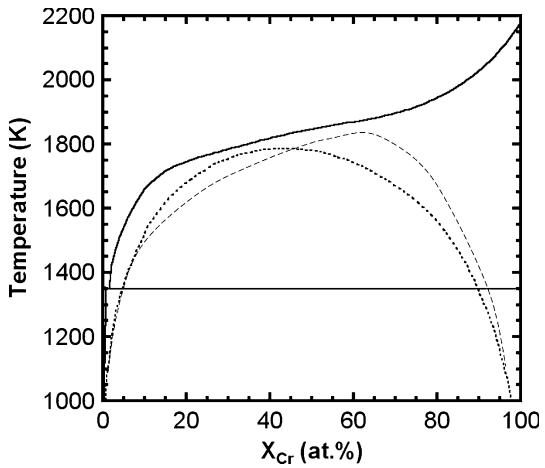

Fig. 5 Illustration of the metastable miscibility gap in the binary Cu–Cr system. The dotted line shows the prediction of a recent thermodynamic study by Jacob et al. [11]. The *dashed line* represents a hypothetical one based on the present results

modified geometry and a Cr-richer critical composition was assumed. As shown by the dashed line of Fig. 5, the hypothesized miscibility gap has a critical composition in-between 60 and 65 at.% Cr, and is skewed remarkably towards the Cr-rich side of the phase diagram. But, at low temperatures, it expands as widely as the calculated one is. Under the assumption of such a skewed miscibility gap, the microstructure of the present samples can be well understood. Since the compositional region for the majority Cu-rich liquid is enlarged at the expenses of the region for the majority Cr-rich liquid, the phase-separated alloy compositions from $x = 5$ to $x = 60$ will show a dispersion of Cr-rich spheroids in the Cu-rich matrix after solidification, as was seen in Fig. 2. As to the microstructure of the alloy compositions with $x = 65$ and 70, a satisfactory explanation can be produced by further considering the thermal history and collision-induced deformation of the bulk samples. As shown in Fig. 5, the hypothetical miscibility gap is closer to the stable liquidus of the two Cr-rich alloy compositions ($x = 65$ and 70) than the calculated one is. It is implied that a smaller critical bulk undercooling was required for triggering of liquid phase separation. Furthermore, the higher liquidus of the two alloy compositions allowed the samples to be cooled at a higher rate than that of the low Cr samples at the first cooling stage. For the two reasons, liquid phase separation in those samples was likely to have started during free fall. After being quenched onto the chill substrate, those samples were cooled at a lower rate than that of the other samples, as was explained in the preceding section. Consequently, they might have experienced a much longer phase separation process, during which the spheroids of the minority phase, namely the Cu-rich liquid, were coarsened, and reached a size of the order of ten micrometers. Upon colliding with the chill substrate, the bulk samples were deformed and spread into the disk-like geometry due to a large impact force. A laminar flow was probably excited in the deformed samples, which forced both the coarsened Cu-rich spheroids and the Cr-rich matrix to be elongated in the flow direction. During solidification, a banded microstructure was frozen in, as was observed in Fig. 3. Actually, the ellipsoidal morphology of the coarse Cr-rich spheroids in medium Cr samples (see Fig. 2d) was formed by the same mechanism. In addition, the formation of shrinkage holes in high Cr samples could be related to a small volume fraction and a lower melting point of the separated Cu-rich liquid. In spite of the identically small volume fraction, the Cr-rich liquid phase in low Cr samples was solidified first because of a higher liquidus, and hence, the shrinkage holes left could be filled in by the low-melting Cu-rich liquid before the samples were fully solidified.

As to the reason for the skewed miscibility gap, it might be related to oxygen impurity dissolved in the levitated samples, which was introduced either by the raw materials or by the argon atmosphere. According to the results of the chemical analysis, the oxygen concentration of the present samples reached a level of few hundred ppms in mass fraction. Such a level of oxygen impurity might have altered the heat of mixing of liquid alloys, leading to an asymmetric miscibility gap and a shift of the liquidus as well. In literature, the same speculation actually has been suggested to account for the observations of the stable miscibility gap under impure experimental conditions [7]. Probably the oxygen level of the present samples was not high enough, and hence, the miscibility gap remained below the liquidus. The influence of the impurity oxygen on the metastable miscibility gap will be investigated later. Apart from the oxygen impurity, the skewed miscibility gap might be related to the modified subregular behavior of the undercooled liquid. In other words, the excess free energy of the liquid phase in undercooled regions might have an expression differing from that proposed by Jacob et al. [11]. To verify this hypothesis, high-accuracy measurements of the heat of mixing on the undercooled liquid need to be performed, which, however, remain difficult.

Conclusions

Electromagnetically levitated Cu–Cr alloy melts containing 5–70 at.% Cr have been splat-quenched onto a chill substrate. The microstructure of the samples has been found to depend on alloy composition. The alloys containing 5–60 at.% Cr showed a droplet-shaped microstructure, whereas those containing 65 and 70 at.% Cr showed a banded microstructure. The observation of the two types of microstructure suggested the existence of a broad miscibility gap in the undercooled liquid, thus verifying the prediction of a recent thermodynamic study of the Cu–Cr system. However, the metastable miscibility gap has been supposed to have a Cr-rich critical composition and a skewed geometry.

Acknowledgement This work is financially supported by the Natural Science Foundation of China under grant No. 50571025.

References

1. Hindrichs G (1908) Z Anorg Chem 59:420
2. Siedschlag E (1923) Z Anorg Chem 131:173
3. Leonov M, Bochvar N, Ivancheko V (1986) Dokl Akad Nauk SSSR 290:888
4. Müller R (1988) Siemens Forsch-u Entwickl-Ber Bd 17:105
5. Timberg L, Toguri JM (1982) J Chem Thermodyn 14:193
6. Kuznetsov GM, Fedorov VN, Rodnyanskaya AL (1977) Izv Vyssh Uchenbn Zaved Tsvetn Metall 3:84
7. Chakrabarti DJ, Laughlin DE (1984) Bull Alloy Phase Diagrams 5:59

8. Hämäläinen M, Jääskeläinen K, Luoma R, Nuotio M, Taskinen P, Teppo O (1990) Calphad 14:125
9. Zeng K, Hämäläinen M (1995) Calphad 19:93
10. Li D, Robinson MB, Rathz TJ (2000) J Phase Equilib 21:136
11. Jacob KT, Priya S, Waseda Y (2000) Z Metallkd 91:594
12. Cooper KP, Ayers JD, Malzahn Kampe JC, Feng CR, Locci IE (1991) Mater Sci Eng A 142:221
13. Sun Z, Zhang C, Zhu Y, Yang Z, Ding B, Song X (2003) J Alloys Compd 361:165
14. Zhou ZM, Wang YP, Gao J, Kolbe M (2005) Mater Sci Eng A 398:318
15. Gao J, Wang YP, Zhou ZM, Kolbe M (2007) Mater Sci Eng A 449–451:654
16. Liu W, Wang GX, Matthys EF (1995) Int J Heat Mass Transf 38:1387
17. Cao CD, Görler GP, Herlach DM, Wei B (2002) Mater Sci Eng A 325:503
18. Curiotto S, Greco R, Pryds NH, Johnson E, Battezzati L (2007) Fluid Phase Equilib 256:132